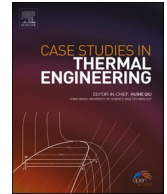




ELSEVIER

Contents lists available at [ScienceDirect](https://www.sciencedirect.com)

## Case Studies in Thermal Engineering

journal homepage: <http://www.elsevier.com/locate/csited>

## Acoustic streaming effect on flow and heat transfer in porous tissue during exposure to focused ultrasound

Teerapot Wessapan<sup>a</sup>, Phadungsak Rattanadecho<sup>b,\*</sup><sup>a</sup> School of Aviation, Eastern Asia University, Pathumthani, 12110, Thailand<sup>b</sup> Center of Excellence in Electromagnetic Energy Utilization in Engineering (CEEE), Department of Mechanical Engineering, Faculty of Engineering, Thammasat University (Rangsit Campus), Pathumthani, 12120, Thailand

## ARTICLE INFO

## Keywords:

Focused ultrasound  
 Porous media  
 Heating  
 Porous tissue  
 Heat transfer

## ABSTRACT

High-intensity focused ultrasound (HIFU) is a minimally invasive technique of regional treatment in which ultrasound waves are focused on targeted tissue. Nevertheless, the precise localization of the target area of HIFU ablation remains challenging. This study investigated acoustic pressure, fluid flow, and heat transfer in porous tissue during exposure to HIFU. The effects of the heat transfer model, tissue permeability, and exposure time on fluid flow and temperature distribution in the tissue were numerically investigated. Additionally, the heating-region shape and heating position were studied. The acoustic pressure, fluid flow, and temperature distributions in the porous tissue during exposure to HIFU were calculated using the numerical simulation of acoustic wave propagation and heat transfer models. The heat transfer models used were formulated based on the conventional bioheat model and porous media theory. With the porous media model, the temperature distributions were observed to be different from those of the conventional bioheat model; this was caused by the acoustic streaming effect. Permeability affected the flow pattern and temperature distribution in the tissue. In particular, tissue permeability also has a significant effect on the position of the target area and lesion shape within the tissue.

## 1. Introduction

High-intensity focused ultrasound (HIFU) ablation is a non-invasive treatment technology that uses focused ultrasound to generate intense heating areas to destroy targeted tissue. HIFU ablations use the heat effect resulting from acoustic energy absorbed by tissue; the technology has been used to treat several tumors including prostate, liver, breast, kidney, sarcoma, and uterine fibroids [1]. Additionally, HIFU may be used for cosmetic applications to treat several cosmetic imperfections such as tightening loose skin, lifting, and body contouring [2,3]. However, the main disadvantage of HIFU is that treatment may cause injury to the surrounding normal tissue. The reason for the injury is the displacement of the focus position and the shape of the coagulative necrosis [4]. Many factors significantly affect this displacement, including transducer design parameters and the tissue acoustic and thermal characteristics. The precise targeting of tissue destruction is challenging and remains a key aspect of treatment planning. Without efficient treatment planning and dose delivery assessment, HIFU ablation may damage surrounding normal tissues along with the targeted ones. The focus of treatment planning is to precisely calculate the energy dose of the treatment to the target tissue; this dose is expressed in seconds of heating at the temperature required to obtain equivalent effects in biological tissues [5]. Consequently, the realistic modeling of the

\* Corresponding author.

E-mail addresses: [teerapot@yahoo.com](mailto:teerapot@yahoo.com) (T. Wessapan), [ratphadu@engr.tu.ac.th](mailto:ratphadu@engr.tu.ac.th) (P. Rattanadecho).<https://doi.org/10.1016/j.csited.2020.100670>

Received 6 April 2020; Received in revised form 26 May 2020; Accepted 27 May 2020

Available online 30 May 2020

2214-157X/© 2020 The Authors. Published by Elsevier Ltd. This is an open access article under the CC BY-NC-ND license

<http://creativecommons.org/licenses/by-nc-nd/4.0/>.

actual transport phenomena associated with heat deposition during HIFU ablation is required to enable the accurate characterization of HIFU fields for effective treatment planning and successful treatment outcomes.

Mathematically modeling the heat transfer in biological tissue is important when investigating the effect of external heat sources such as HIFU and in predicting the success of the overall treatment outcome. Mathematical models of heat transfer in biological tissue have been continuously developed over time and have been used specifically in treatment planning and various applications. The bioheat model of a blood-perfused tissue was first proposed by Pennes [6] based on the heat diffusion model. Because of the simplification of Pennes' bioheat model, some researchers modified and extended it [7,8]. Kundu and Dewanjee proposed non-Fourier bioheat transfer equations for skin tissue that is exposed to various heating conditions [9]. Some researchers proposed a countercurrent heat exchange system in arterial-venous blood vessels [10,11]. In practice, human tissue is composed primarily of water and can be considered a blood-saturated tissue represented by a porous medium. Recently, interest has increased in using porous media theory to model transport phenomena in living tissues. A porous media approach is likely to be more appropriate for modeling transport phenomena in biological tissues because it requires fewer assumptions, as was stressed by Dhall, Halder, and Datta [12]. Another study investigated the hydrodynamics of blood flow in a porous medium [13]. Many research groups have attempted to describe advanced numerical models for various HIFU treatment planning scenarios and techniques [14–19]. Gupta and Srivastava conducted the transient thermal analysis of multi-layered media subjected to HIFU [20,21]. Our research group conducted a sophisticated thermal modeling of human tissues and organs in various applications such as (a) microwave ablation [22], (b) laser-assisted ablation [23], (c) focused ultrasound ablation [24], and (d) effects of electromagnetic fields on the brain [25,26], eyes [27,28], organs [29–31], and tissues [32]. Recently, we conducted a numerical simulation of the temperature distribution in a deformed vascular tissue during HIFU ablation [24].

The use of porous media theory has been proposed in several biomedical studies [12–15,27,28,32]. However, most studies on treatment planning have not considered the porous media approach, particularly in HIFU treatment planning, although it is a more realistic approach than the conventional bioheat model. Therefore, the actual thermo-physiological responses of biological tissues subjected to HIFU ablation have not yet been modeled completely because of the physical complexity associated with transport in biological tissue and acoustic propagation.

This study used the porous media theory to analyze the acoustic pressure field, fluid flow, and temperature distribution in a biological tissue subjected to a HIFU ablation. In the tissue model, the effects of the heat transfer model, tissue permeability, and

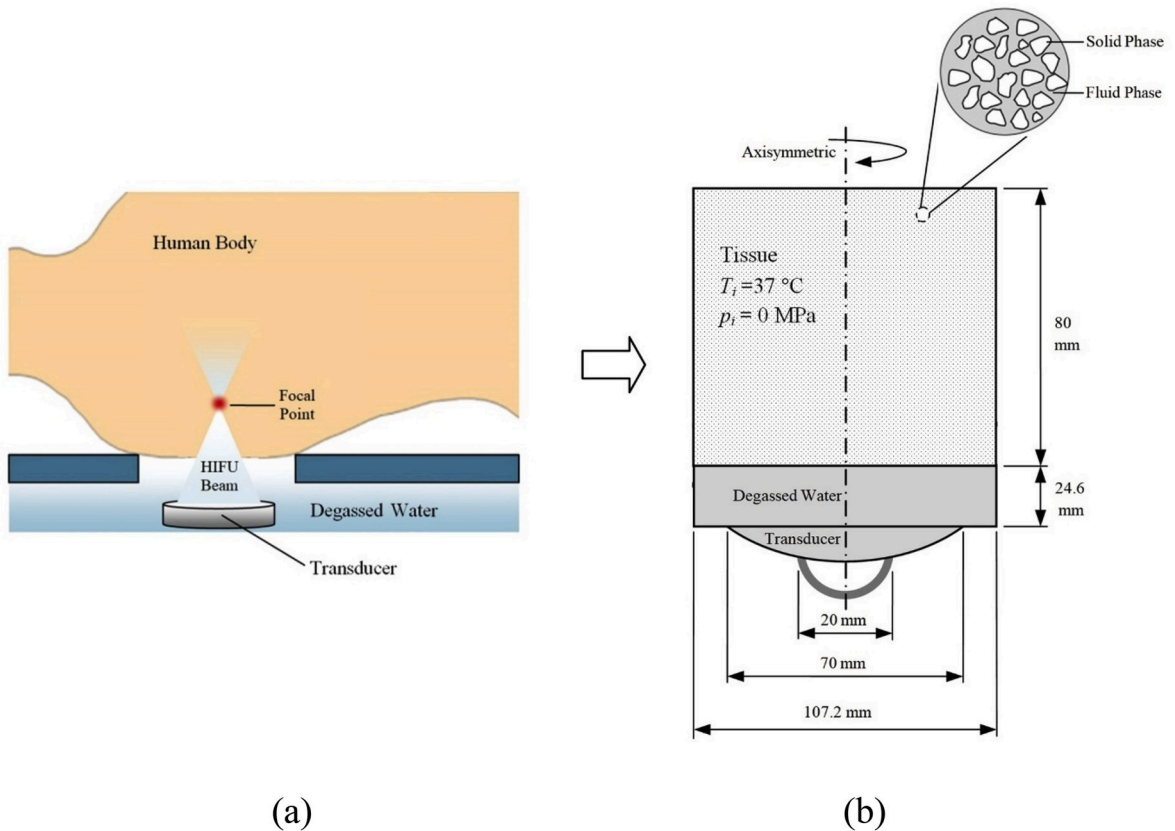


**Fig. 1.** Physical model of the problem:  
 (a) Schematic diagram of HIFU treatment,  
 (b) Model details.

exposure time on fluid flow and temperature distribution in the porous tissue were numerically investigated. The acoustic pressure field, fluid flow, and temperature distributions in the tissue during exposure to HIFU ablation were calculated using the numerical simulations of the acoustic wave propagation, momentum, continuity, and energy equations. The calculated temperatures of the conventional bioheat and porous media models were compared. This was one of the very few studies in the context of HIFU whose numerical simulations considered the permeability effect of the biological tissues. The results of this study can be useful for improving the parameters that must be considered for the local properties of the specific target tissue for effective treatment planning and successful treatment outcomes.

## 2. Formulation of the problem

HIFU is a minimally invasive technique for regional treatment in which ultrasound waves are focused on a targeted tissue to heat it to its coagulation temperature. Fig. 1a shows the schematic of HIFU producing high localized temperatures deep within the body. The main disadvantage of using the HIFU technique is that it may result in injury to the normal tissue surrounding the tumor. The reason for the injury is the displacement of the focus position and the shape of the coagulative necrosis that might be caused by the acoustic streaming effect or inaccurate treatment planning. Thus, the precise targeting of the lesion is challenging and becomes a key concern. For a comprehensive approach to the transport phenomena in a tissue caused by HIFU exposure, we proposed a coupled acoustic-thermal-fluid model of porous tissue. The proposed model was used to study the acoustic streaming effect of HIFU exposure on the transport phenomena in the tissue.

## 3. Methods and model

The study focused on the effect of acoustic streaming on flow and heat transfer in porous tissue during exposure to focused ultrasound. The first step to understand the effects of ultrasonic energy exposure during HIFU ablation was to calculate the induced acoustic pressure and its distribution. Thereafter, the energy absorbed, which resulted in a temperature increase and related transport phenomena in the tissue, was investigated. This study considered the induced acoustic pressure occurring in the ultrasonic field and transport consequences of HIFU exposure. The values of the parameters selected for the study were based on tumor ablation. The results were used as a guideline in the implications of the threshold for thermal damage to the tissue.

### 3.1. Physical model

A homogeneous tissue model was considered to study the interaction between HIFU and the porous tissue as well as its transport phenomena. Fig. 1b illustrates the physical model and its details, in which an interaction between the tissue and acoustic waves occurs. The tissue model used in this study was considered a fluid-saturated tissue that can be represented by a porous medium. The porous tissue model considered could be separated into vascular (fluid phase) and extra-vascular (solid phase) regions [13] (Fig. 1b). In this study, a 2D axisymmetric model represented a vertical cross-section of the 3D model that was considered to minimize the computational time while maintaining resolution. In the model, the porous tissue and transducer were immersed in degassed water in a closed container. The ultrasound source was a single-element, spherically focused, piezoelectric transducer with a 70-mm-diameter aperture of and a 20-mm-diameter hole in the center. The transducer had a focal length of 62.64 mm and a frequency of 1.0 MHz. The tissue model was a cylinder with a diameter of 107.2 mm and a length of 80 mm. The degassed water was 24.6 mm from the interface. The tissue was homogeneous and acoustically and thermally isotropic with constant thermal properties. The porous tissue was saturated with fluid and no large vessel existed in the tissue. No chemical reaction and phase change occurred within the tissue.

### 3.2. Equation for acoustic wave propagation analysis

The acoustic pressure within the tissue was determined by solving the acoustic wave equation. The problem was simplified by modeling the acoustic wave propagation in a 2D axisymmetric geometry, and the model assumed that the acoustic properties of the tissue were uniform and constant. The wave equation governing the acoustic field can be expressed in a simplified form by the axisymmetric Helmholtz equation in cylindrical coordinates, which mathematically describe the propagation of acoustic waves through a medium given by the following equation [16]:

$$\frac{\partial}{\partial r} \left[ -\frac{r}{\rho} \left( \frac{\partial p_s}{\partial r} \right) \right] + r \frac{\partial}{\partial z} \left[ -\frac{1}{\rho} \left( \frac{\partial p_s}{\partial z} \right) \right] - \left[ \left( \frac{\omega}{c_0} \right)^2 \right] \frac{r p_s}{\rho} = 0 \quad (1)$$

where  $p_s$  is the acoustic pressure (Pa),  $\omega$  is the angular frequency (rad/s),  $\rho$  is the density ( $\text{kg/m}^3$ ),  $c_0$  is the speed of sound (m/s), and  $r$  and  $z$  are the radial and axial coordinates, respectively.

#### 3.2.1. Boundary condition for acoustic wave propagation analysis

In the axisymmetric model, the axial symmetry boundary condition was applied at the symmetry axis  $r = 0$ :

$$\frac{\partial p_{s,r}}{\partial r} = 0 \quad (2)$$

The inward normal acceleration ( $a_n$ ) ( $\text{m/s}^2$ ), which represents an external source term, was applied to the surface of the acoustic transducer.

$$-n \cdot \left[ -\frac{1}{\rho_c} (\nabla p_s - q) \right] = a_n \quad (3)$$

Because the tissue phantom was placed in the tissue container, the walls were assumed to be rigid; thus, the outer sides of the domain were considered as sound-hard boundary conditions:

$$-n \cdot \left[ -\frac{1}{\rho_c} (\nabla p_s - q) \right] = 0 \quad (4)$$

where  $q$  is the dipole source ( $\text{N/m}^3$ ) and  $n$  is the normal vector.

In this study, the dipole source term was assumed to be zero.

### 3.3. Equations for heat transfer and flow analysis

When an acoustic wave is transmitted through biological tissue, it experiences a loss of kinetic energy via conversion into heat due to absorption. To comprehensively evaluate the problem stated earlier in Section 2, we investigated the coupled effect of the acoustic wave propagation, fluid flow, and unsteady heat transfer of the porous tissue. To simplify the problem, we considered the following assumptions:

- 1 The tissue had constant thermal properties.
- 2 No phase change of substance occurred during the process.
- 3 No chemical reaction occurred in the tissue.
4. The tissue was a homogeneous, thermally isotropic, and fluid-saturated porous media.

This study considered two types of thermal models to investigate the transport process of the tissue when exposed to HIFU:

#### 3.3.1. Model I: The conventional bioheat model

The Pennes' bioheat model [6] is one of the earliest models of heat transfer in biological tissue. It has been extensively used to model heat transfer in biological tissue because of its simplicity and minimal data requirements. The bioheat model considers heat transport in tissue due to heat conduction, blood perfusion, and metabolic heat generation. The transient bioheat model describes the heat transfer characteristics of the biological tissue based on the classical Fourier's law; the model can be expressed as

$$\rho C \frac{\partial T}{\partial t} = \nabla \cdot (k \nabla T) + \rho_b C_b \omega_b (T_b - T) + Q_{met} + Q_{ext} \quad (5)$$

where  $\rho$  is the density of tissue ( $\text{kg/m}^3$ ),  $T$  is the tissue temperature ( $^{\circ}\text{C}$ ),  $T_b$  is the blood temperature ( $^{\circ}\text{C}$ ),  $t$  is the time,  $k$  is the thermal conductivity of tissue ( $\text{W/m K}$ ),  $C$  is the tissue heat capacity ( $\text{J/kg K}$ ),  $C_b$  is the blood heat capacity ( $\text{J/kg K}$ ),  $\rho_b$  is the blood density ( $\text{kg/m}^3$ ),  $\omega_b$  is the blood perfusion rate,  $Q_{met}$  is the metabolic heat generation ( $\text{W/m}^3$ ), and  $Q_{ext}$  is the external heat source ( $\text{W/m}^3$ ).

#### 3.3.2. Model II: The porous media model

The porous media approach is probably the most practical approach to model the transport phenomena in biological tissue because it has fewer assumptions than the conventional bioheat model. In the porous media model, heat transfer in the tissue is modeled as a fluid-saturated porous medium and coupled with the acoustic wave pressure equation that describes acoustic propagation characteristics in any medium. The Brinkman-extended Darcy model [33] is used to characterize the fluid transport within the porous tissue. The equations governing fluid flow in the porous tissue are as follows:

Continuity equation:

$$\nabla \cdot u = 0 \quad (6)$$

Momentum equation:

$$\left( \frac{\rho}{\varepsilon_p} \right) \frac{\partial u}{\partial t} + \left( \frac{\mu}{\kappa} \right) u = -\nabla p + \nabla \cdot \left[ \left( \frac{1}{\varepsilon_p} \right) \left( \mu \left( \nabla u + (\nabla u)^T \right) \right) \right] + F \quad (7)$$

where  $\rho$  is the tissue density ( $\text{kg/m}^3$ ),  $\kappa$  is the tissue permeability ( $\text{m}^2$ ),  $u$  is the flow velocity ( $\text{m/s}$ ),  $p$  is the pressure ( $\text{Pa}$ ),  $\mu$  is the dynamic viscosity ( $\text{N.s/m}^2$ ),  $T$  is the tissue temperature ( $\text{K}$ ),  $\varepsilon_p$  is the tissue porosity, and  $F$  is the body force induced by acoustic streaming ( $\text{N/m}^3$ ), which can be expressed as

$$F = \frac{2\alpha}{c_0} I \quad (8)$$

The governing equation for transient heat transfer in the tissue is as follows:

Energy equation:

$$(\rho C)_{eff} \frac{\partial T}{\partial t} - \nabla \cdot (k_{eff} \nabla T) = -(\rho C)_b u \cdot \nabla T + Q_{met} + Q_{ext} \quad (9)$$

where

$$(\rho C)_{eff} = (1 - \varepsilon_p)(\rho C)_s + \varepsilon_p(\rho C)_b \quad (10)$$

is the overall heat capacity per unit volume of the tissue, and

$$k_{eff} = (1 - \varepsilon_p)k_s + \varepsilon_p k_b \quad (11)$$

is the overall thermal conductivity. The subscripts *eff*, *s*, and *b* correspond to the effective value, solid tissue phase, and blood phase, respectively.

The external heat source term is equal to the absorbed heat generated by the intense acoustic field (the absorbed acoustic energy), which is defined as

$$Q_{ext} = 2\alpha I \quad (12)$$

where  $\alpha$  is the tissue's acoustic absorption coefficient ( $\text{m}^{-1}$ ),  $p_s$  is the acoustic pressure (Pa), and  $I$  is the acoustic intensity ( $\text{W}/\text{m}^2$ ).

### 3.3.2. Boundary conditions for heat transfer and flow analysis

Only the heat transfer and flow analysis were considered in the tissue model. The temperature of the tissue's exterior surfaces was assumed to be constant at  $37^\circ\text{C}$ . For flow analysis, the external boundaries of the tissue model were represented by the open boundary condition where fluid can flow in and out of the computational domain.

$$n \cdot \left[ -p2i + \left( \frac{1}{\varepsilon_p} \right) \mu \left( \nabla \cdot u + (\nabla \cdot u)^T \right) \right] = -f_0 \cdot n \quad (13)$$

where  $n$  is the normal vector of the boundary,  $p$  is the pressure (Pa),  $u$  is the velocity (m/s),  $f_0$  is normal stress ( $\text{N}/\text{m}^2$ ),  $i$  is the identity matrix,  $\mu$  is the dynamic viscosity ( $\text{Pa}\cdot\text{s}$ ), and  $\rho$  is the density ( $\text{kg}/\text{m}^3$ ).

The surface that was exposed to ultrasound was considered as no-slip boundary condition.

$$u = 0 \quad (14)$$

The initial temperature was assumed to be uniform over the entire model.

$$T(t_0) = 37^\circ\text{C}. \quad (15)$$

The outer surface of the tissue model remained at a constant temperature of  $37^\circ\text{C}$ .

### 3.4. Calculation procedure

The finite element method (FEM) was used to numerically solve the system of governing equations and initial and boundary conditions. The adaptive mesh refinement method was employed to solve the numerical problem. The computational problem was solved via COMSOL<sup>TM</sup> Multiphysics to study the phenomena that occurred in the tissue model during exposure to HIFU.

## 4. Results and discussion

The acoustic pressure, flow field, and temperature distributions in the porous tissue during exposure to HIFU were obtained by the numerical simulation of the acoustic wave propagation, momentum, continuity, and energy equations. The properties of muscle tissue

**Table 1**  
Thermal properties and acoustic properties of the tissue [34].

Tissue properties	Values
Tissue density ( $\rho$ )	1,090 $\text{kg}/\text{m}^3$
Heat capacity of tissue ( $C$ )	3,421 $\text{J}/\text{kg K}$
Heat capacity of blood ( $C_b$ )	3,617 $\text{J}/\text{kg K}$
Thermal conductivity of tissue ( $k$ )	0.49 $\text{W}/\text{m K}$
Density of blood ( $\rho_b$ )	1,049 $\text{kg}/\text{m}^3$
Blood perfusion rate ( $\omega_b$ )	0.0001 $\text{s}^{-1}$
Tissue porosity ( $\varepsilon_p$ )	0.4
Acoustic absorption coefficient ( $\alpha$ )	7.11 $\text{m}^{-1}$
Speed of sound ( $c_c$ )	1,588.4 $\text{m}/\text{s}$

were used as the basis of modeling to study the acoustic streaming effect in tissue. The acoustic and thermal properties of the tissue shown in Table 1 were obtained directly from the consolidated literature review of Hasgall et al. [34]. The exposure condition considered in this study referred to the tissue necrosis at a reference temperature of 43 °C [5]. The effects of the heat transfer model, exposure time, and tissue permeability on distributions of acoustic pressure, fluid flow, and temperature within the tissue were numerically investigated using two models, namely, the conventional bioheat (Model I) and porous media (Model II) models.

#### 4.1. Verification of the model

The numerical model presented here was verified by validating the simple scenario of the simulated result against the results with the same geometric model obtained by Huang et al. [19]. The temperature increase in the homogeneous tissue model from exposure to HIFU was determined using the conventional bioheat model. In the validation, the transducer used operated at a frequency of 1.1 GHz. The tissue had a thermal conductivity of 0.59 W/m·K, a specific heat of 3700 J/kg·K, a density of 1045 kg/m<sup>3</sup>, a sound speed of 1550 m/s, an acoustic absorption coefficient of 10 m<sup>-1</sup>, and its outer surface maintained a constant temperature of 37 °C. Fig. 2 shows the characteristics of heating and cooling curves for an exposure time of 1 s and cooling time of 4 s. The figure indicates that the values of the temperature increase in the tissue model in the numerical results of this study and that of Huang exhibited good agreement. The agreement from the comparison indicated the accuracy of the proposed numerical model. Thus, the numerical model can be used to represent phenomena occurring due to the interaction of the HIFU with the tissue.

#### 4.2. Pressure distribution

Numerical modeling has been used in characterizing pressure fields created by acoustic transducer. In this study, the tissue model was exposed to HIFU at a frequency of 1.0 GHz to illustrate the pressure distribution in the tissue domain. Fig. 3a shows the acoustic pressure distribution in the axial distance from the acoustic source where the peak of acoustic pressure was highest at the focal point of  $62.64 \pm 5$  mm. Fig. 3b shows the acoustic pressure distribution in the radial distance where acoustic pressure decreased rapidly with radial distance from the center of the focal area. We observed that the highest values of pressure fields occurred at the focal area of the tissue domain throughout the process. At the radiated power of 15 W, the maximum acoustic pressure in the tissue domain was 3.5 MPa.

#### 4.3. Effect of different heat transfer models

This study considered two types of thermal models, the conventional bioheat model (Model I) and porous media model (Model II), to investigate the transport process of the tissue when exposed to HIFU. This subsection describes the numerical investigation of the effect of different heat transfer models on the temperature profiles in the tissue model at various exposure times. The conventional bioheat model used in this study was based on Fourier's law. In the porous media model, heat transfer in the tissue was modeled as a fluid-saturated porous medium (blood-saturated tissue). This model adopted the Brinkman-extended Darcy equation to represent the fluid transport within the porous tissue. The heat transfer models considered were coupled with the acoustic wave pressure equation that describes acoustic propagation characteristics in any medium. The calculated temperature of the conventional bioheat model and

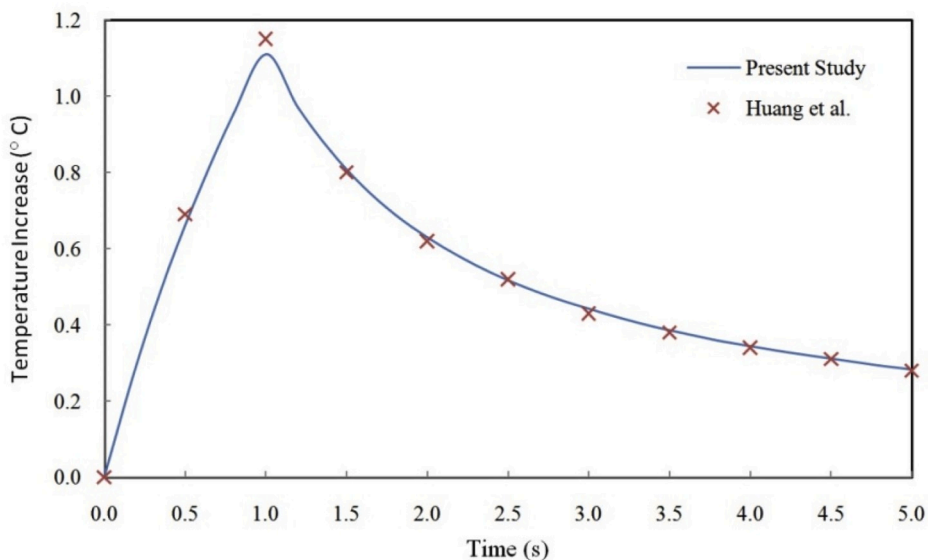
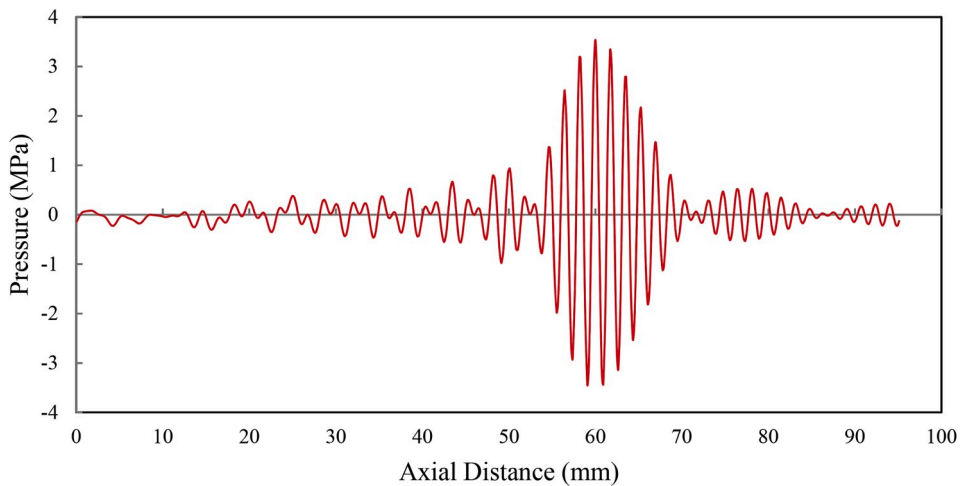
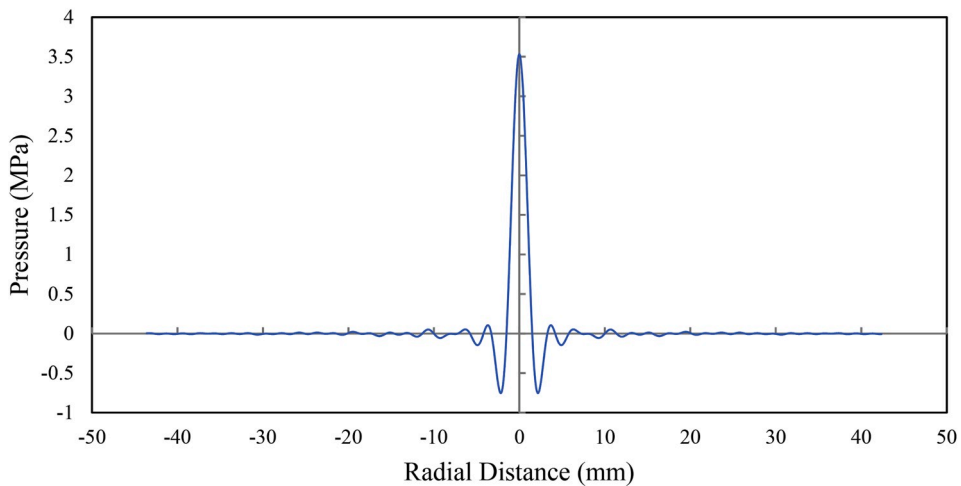


Fig. 2. Comparison between temperature increase-time profiles obtained from this numerical study and obtained by Huang et al. [19].



(a)



(b)

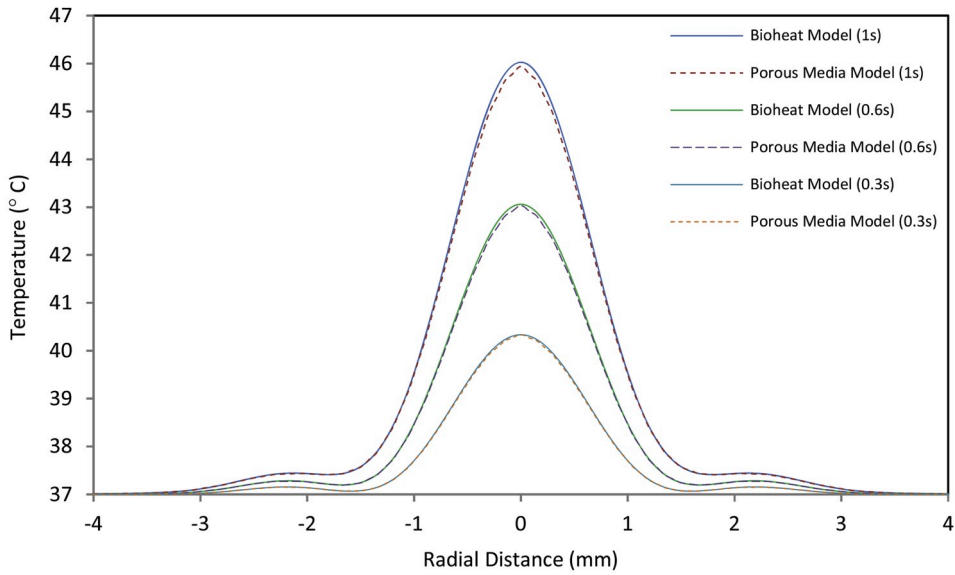
**Fig. 3.** Computed acoustic pressure profile in the tissue:

- (a) in axial distance,
- (b) in radial distance.

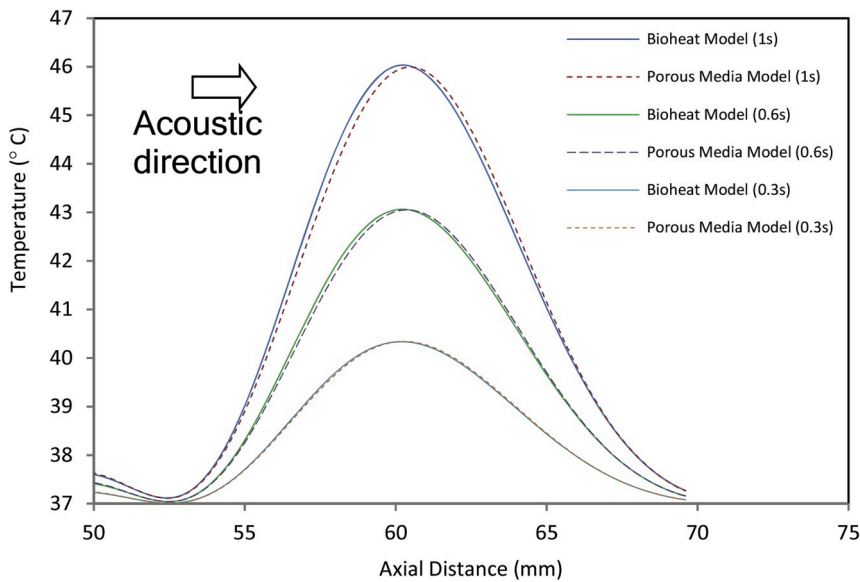
was compared to that of the porous media model, which considered the convection flows arising from acoustic streaming.

Because this study focused on the HIFU-induced heating in the targeted porous tissue, the effect of environmental temperature change was neglected to focus on the interaction between HIFU and porous tissue and the correlation between acoustic pressure, fluid flow, and heat transfer mechanism. The porosity of the porous tissue ( $\epsilon_p$ ) used was 0.4, the permeability of a porous tissue ( $\kappa$ ) here was assumed to be  $5 \times 10^{-11} \text{ m}^2$  based on the experimental data of Fahlgren et al. [35], and the initial fluid velocity was assumed to be zero. In the porous media model, a coupled acoustic-thermal-fluid model of fluid-saturated porous tissue was established to illustrate the acoustic streaming effect of HIFU exposure on transport phenomena in the tissue. Because of the coupled effects, the acoustic energy transmitted via acoustic pressure, shown in Fig. 3, was converted into heat by absorption of the tissue.

Fig. 4 shows the comparisons of the temperature profiles in the tissue of the bioheat and porous media models at various exposure times at the acoustic power of 15 W plotted in the radial direction at the focal point cross-section (Fig. 4a) and axial direction from the acoustic source (Fig. 4b). With the porous media model, the temperature profiles and maximum points of temperature were observed to be different from those of the conventional bioheat model because of the strong convection that occurred within the porous media model. The maximum temperature difference at the focal point between the two models was approximately 1%. In the radial direction



(a) radial direction



(b) axial direction

Fig. 4. Temperature profiles in the tissue at various exposure times plotted in (a) radial direction (b) axial direction.

(Fig. 4a), the temperature profiles of the porous media model were observed to be slightly lower than those of the conventional bioheat model. In the axial direction (Fig. 4b), the maximum temperature points of the porous media model appeared to shift slightly from the conventional bioheat model according to the flow direction induced by the streaming effect of the acoustic wave (Fig. 5).

Fig. 5 shows the instantaneous velocity vector field and the contour lines of flow velocity in the tissue at the exposure time of 1 s. The acoustic streaming velocity was induced by the absorbed focused ultrasonic energy. Here, the focused ultrasound waves of HIFU induced acoustic streaming velocity to attain a steady-state level at  $5.67 \times 10^{-4}$  m/s within 0.3 s. The velocity gradient associated with the acoustic streaming flow in the tissue was high, particularly near the focal point, and the maximum velocity occurs in the middle of the

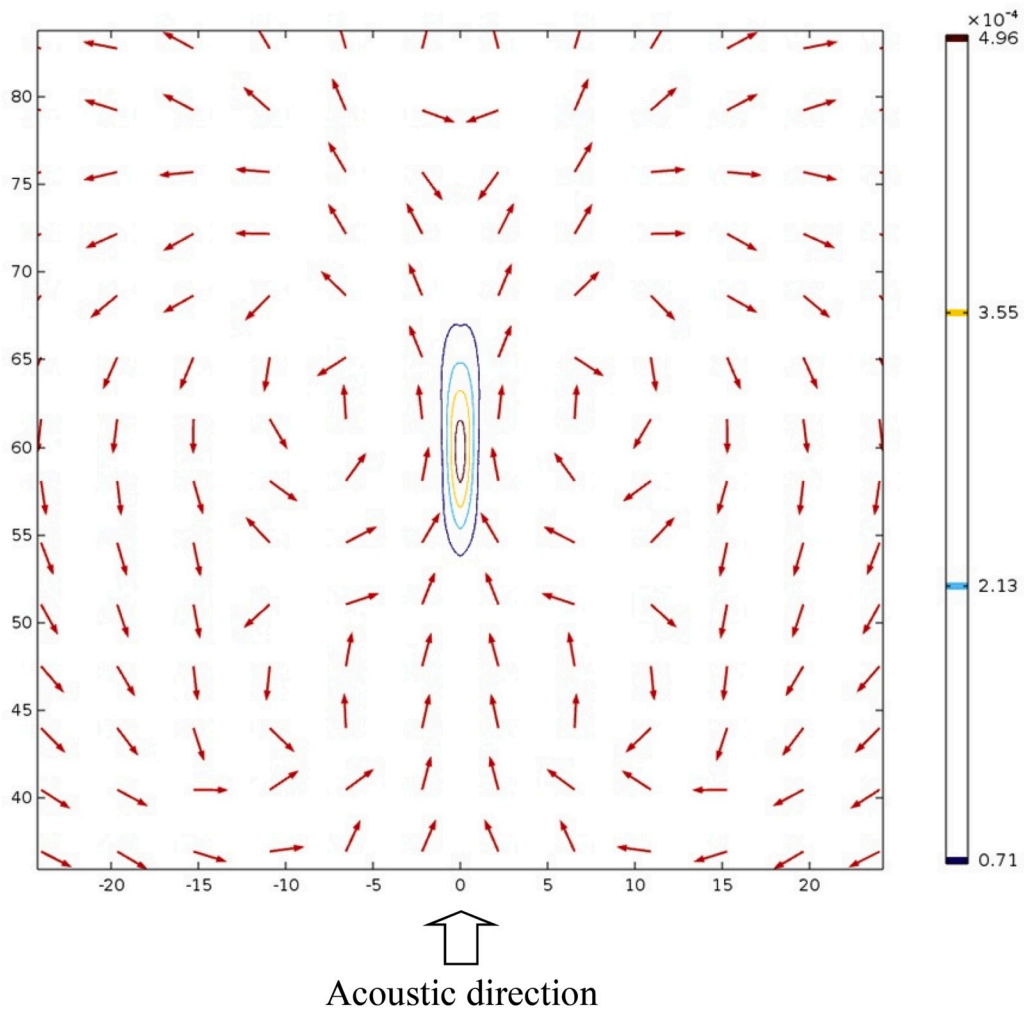
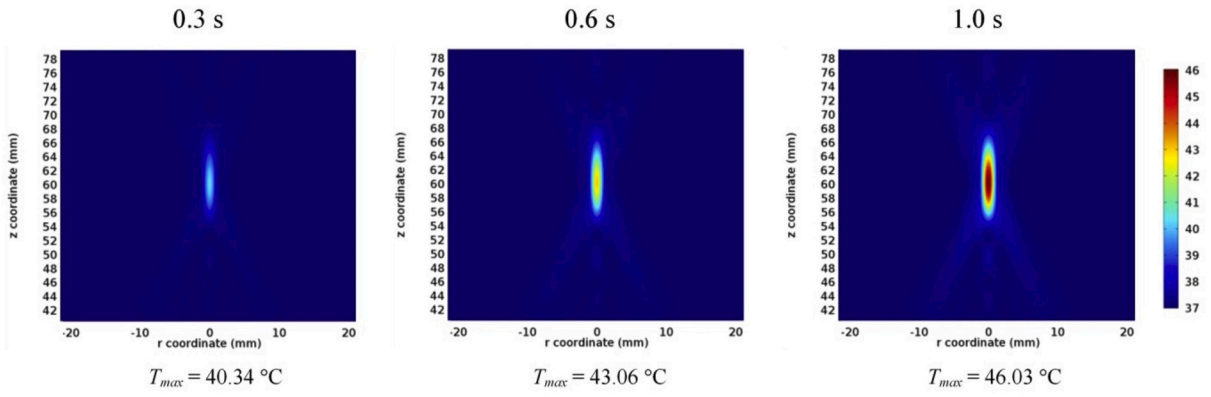


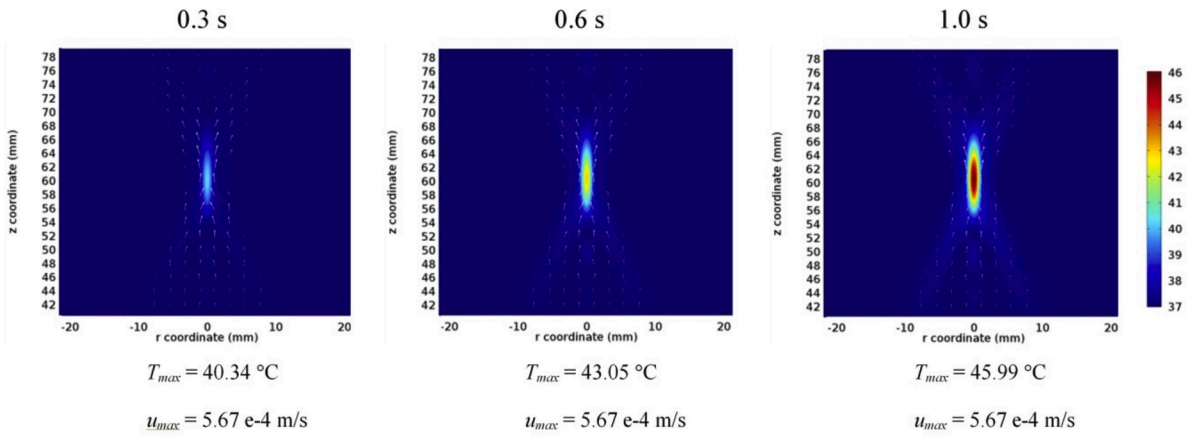
Fig. 5. Instantaneous velocity vector field and the contour lines of flow velocity in the tissue at the exposure time of 1 s.

focal region owing to the mass flowing into the focal region. The figure shows the nearly axial flow pattern near the center of the model around the focal point and the reverse flow at a large distance from the focal point. The velocity increased steeply near the focus. The flow-induced by acoustic streaming was observed to have a marked effect on thermal convection. The fluid flow included in the porous media model contributed to cooling and caused changes in the temperature profile patterns predicted by the model shown in Fig. 4.

Fig. 6 shows the temperature and velocity fields in the tissue at various exposure times calculated using the conventional bioheat model (Fig. 6a) and the porous media model (Fig. 6b). For the tissue exposed to the HIFU for a time, the temperature within the tissue (Fig. 6) increased corresponding to the acoustic pressure (Fig. 3). This was because the absorbed acoustic energy was converted to thermal energy, which increased the tissue temperature. As expected, the longer exposure time contributed to increases in tissue temperature during HIFU ablation. With the conventional bioheat model, the maximum temperatures were 40.34, 43.06, and 46.03 °C for exposure times of 0.3, 0.6, and 1.0 s, respectively. With the porous media model, the maximum temperatures were 40.34, 43.05, and 45.99 °C for exposure times of 0.3, 0.6, and 1.0 s, respectively. The flow in the porous media model had a constant maximum velocity of  $5.67 \times 10^{-4}$  m/s in all scenarios because they attained a steady-state. According to results of the heat-induced coagulative necrosis of tissue from a temperature increase above 43 °C [5], the coagulative necrosis zone exhibited a clear ellipsoidal shape at an exposure of 0.6 s and more at the focal point region. In the porous tissue, the velocity fields were driven by a pressure gradient in the direction of the acoustic streaming and varied according to the pressure field intensity in the tissue (Fig. 3). At 0.3 s, when the temperature gradient was small, no apparent temperature difference was observed between the two heat transfer models. However, from 0.6 s onwards, the highest temperatures calculated from the porous media model were slightly lower than those of the conventional bioheat model. This was due to the dominant effect of acoustic streaming flow at a higher temperature gradient of the porous media model (Fig. 6b). The acoustic streaming flow contributed significantly to decreasing heat accumulation in a high-temperature gradient region of the porous tissue. Since this study was carried out in short exposure time, the resulting temperature increases obtained were small (less than 10 °C). We suggest that temperature-dependent thermal properties should be considered in the case of a higher



(a) Bioheat Model



(b) Porous Media Model

Fig. 6. Temperature and velocity fields in the tissue at various exposure times calculated using (a) the conventional bioheat model (b) the porous media model.

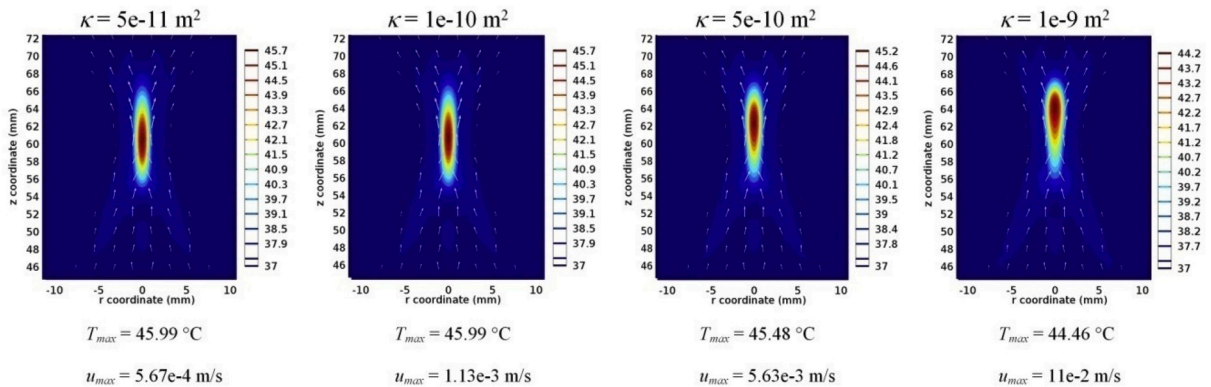


Fig. 7. Temperature and velocity fields of various permeability values in the tissue exposure to the focused ultrasound for 1 s.

temperature threshold with longer exposure time.”

#### 4.4. Effect of tissue permeability

The biological tissue can be represented as a fluid-saturated porous tissue matrix including cells and interstices. The porous tissue model considered can be separated into the vascular (fluid phase) and extra-vascular (solid phase) regions. Tissue permeability ( $\kappa$ ) is a physical property related to tissue structures, and it represents the ability of a porous tissue to transmit fluids. Tissue permeability depends on the tissue void ratio and the volumetric fraction of the pore volume (saturation). Four different tissue permeability values, namely,  $5\text{e-}11$ ,  $1\text{e-}10$ ,  $5\text{e-}10$ , and  $1\text{e-}9\text{ m}^2$  were used to study the transport phenomena induced by HIFU exposure within the tissue model.

Fig. 7 shows the temperature and velocity fields of various permeability values in the tissue exposure to the 15-W HIFU for 1 s. The maximum temperatures were 45.99, 45.99, 45.48, and 44.46 °C for the permeability values of  $5\text{e-}11$ ,  $1\text{e-}10$ ,  $5\text{e-}10$ , and  $1\text{e-}9\text{ m}^2$ , respectively. The maximum fluid flow velocities were  $5.67\text{e-}4$ ,  $1.13\text{e-}3$ ,  $5.63\text{e-}3$ , and  $11.0\text{e-}2\text{ m/s}$  for the permeability values of  $5\text{e-}11$ ,  $1\text{e-}10$ ,  $5\text{e-}10$ , and  $1\text{e-}9\text{ m}^2$ , respectively. The fluid flow in the tissue that was driven by acoustic streaming was observed to vary according to the tissue permeability. The higher value of tissue permeability corresponded to the higher fluid flow velocity in the porous tissue. This was because the higher value of tissue permeability enabled higher flow rates through the void space. The comparison of the temperature-induced in different values of tissue permeability indicated that the peak temperature of each scenario did not precisely occur in an identical position. The maximum temperatures of the porous tissue with lower permeability values of  $5\text{e-}11$  and  $1\text{e-}10\text{ m}^2$  occurred in the geometrical focal region, which corresponded to the peak of the pressure shown in Fig. 3. However, the maximum temperatures at higher permeability values of  $5\text{e-}10$  and  $1\text{e-}9\text{ m}^2$  exhibited noticeable shifts with the downstream direction of the geometrical focus position along with the increase in the flow velocity. We observed that a higher flow velocity in the higher permeability tissue accompanied a shift downstream of the heating focal spot.

Furthermore, no significant temperature difference was observed between the tissues with lower permeabilities of  $5\text{e-}11$  and  $1\text{e-}10\text{ m}^2$ , while the tissues with higher permeabilities of  $5\text{e-}10$  and  $1\text{e-}9\text{ m}^2$  had a lower maximum temperature than the lower permeability tissues. This was because the higher flow velocities in the higher permeability tissues contributed significantly to decreasing heat accumulation in the tissue in a high-temperature gradient region.

Fig. 7 indicates that the flow velocity in the higher-permeability tissue was higher than that of lower-permeability tissues. The flow velocities were significantly higher near the focal area because of higher-pressure gradients, thus generating a stronger acoustic streaming force that drove fluid flow. For the porous media model, the unsymmetrical heating-region shape occurred noticeably in the higher permeability tissue and the locations occurred were not exactly the geometrical focal spot of the transducer, but rather a few millimeters downstream of the focal zone.

In the lower-permeability tissues ( $\kappa = 5\text{e-}11$  and  $1\text{e-}10\text{ m}^2$ ), the peak temperature occurred at the same position with respect to the position of the peak acoustic pressure shown in Fig. 3. This was because fluid flow in the lower permeability tissues was retarded owing to the flow resistance of the porous tissue structure. Consequently, the fluid flow was virtually motionless, indicating that conduction was a dominant heat transfer mechanism. In the higher permeability tissues ( $\kappa = 5\text{e-}10$  and  $1\text{e-}9\text{ m}^2$ ) with higher flow velocity, the maximum temperature points appeared to shift slightly to the higher position as a result of the flow direction shown in Fig. 5. In this case, the permeability affects the heating patterns and heating positions within the tissue. However, for tissue permeability values of  $5\text{e-}11\text{ m}^2$  or lower, convection induced by acoustic streaming has almost no effect on tissue temperature change and heating position.

## 5. Conclusions

A numerical analysis of the acoustic pressure, fluid flow, and heat transfer in the porous tissue during exposure to HIFU was performed. In this study, the effects of heat transfer model, tissue permeability, and exposure time on flow and temperature distribution in the porous tissue were investigated numerically. Additionally, we investigated the acoustic streaming effect on heating-region shape and heating position. The acoustic pressure, fluid flow, and temperature distributions in the tissue during exposure to HIFU were obtained by the numerical simulation of acoustic wave propagation, momentum, continuity, and energy equations. The heat transfer models used in the investigation were formulated based on the conventional bioheat model and porous media theory.

Consequently, the highest values of pressure fields occurred at the focal area of the tissue domain throughout the process. The acoustic pressure in the axial distance from the acoustic source had the highest value at the focal point of  $62.64 \pm 5\text{ mm}$ , whereas it decreased steeply with increasing radial distance from the focal area. The calculated temperatures of the conventional bioheat and porous media models were compared. The temperature distribution patterns of the two models at a particular time were observed to be different. The highest temperature calculated for the porous media model was slightly lower than that of the conventional bioheat model. This was because a dominant effect of acoustic streaming flow at a higher temperature gradient of the porous media model contributed significantly to the decrease in heat accumulation in the tissue in a high-temperature gradient region. The longer exposure time contributed to increasing the tissue temperature during HIFU ablation.

Furthermore, the tissue permeability had an effect on the temperature distribution in the porous tissue. The higher tissue permeability correlated to the lower temperature increase of the porous tissue. The flow velocities were significantly higher near the focal area because of higher acoustic pressure gradients, thus generating a stronger acoustic streaming force that drove the fluid flow. The higher value of tissue permeability enabled higher flow velocity through the void space. In the low-permeability tissue, the fluid flow was suppressed because of the resistance of the porous medium structure, and the flow was virtually motionless, indicating that conduction was a dominant heat transfer mechanism. For the porous media model, the unsymmetrical heating-region shape occurred

noticeably in the higher-permeability tissue and the heating locations were not exactly at the geometrical focal spot of the transducer, but rather a few millimeters downstream of the focal zone. This was not directly caused by the ultrasound waves but by the acoustic streaming effect. Therefore, the acoustic streaming effect of HIFU has a significant effect on the locations of the target area and lesion shape of the high permeability tissue. We noted that this work is basic research that demonstrates the influence of permeability with higher values than most other tissues. Therefore, the obtained results may not be directly applicable in practical situations.

The results contribute to a better understanding of modeling the temperature distribution within a tissue during HIFU ablation. This can be useful for improving parameters that must be considered for the local properties of the specific target tissue for effective treatment planning and successful treatment outcomes. This paper can be of significant interest to the readers, particularly those working in the related area of hyperthermia using HIFU applications.

### Declaration of competing interest

The authors declare that they have no known competing financial interests or personal relationships that could have appeared to influence the work reported in this paper.

### CRedit authorship contribution statement

**Teerapot Wessapan:** Investigation, Writing - original draft. **Phadungsak Rattanadecho:** Supervision.

### Acknowledgments

The authors gratefully acknowledge the Thailand Research Fund (TRF), the Commission on Higher Education (CHE) (under the TRF contract No. MRG6180277 and RTA5980009), and The Thailand Government Budget Grant.

### Nomenclatures

$a$	acceleration ( $\text{m/s}^2$ )
$C$	specific heat capacity ( $\text{J}/(\text{kg K})$ )
$c_0$	speed of sound ( $\text{m/s}$ )
$F$	body force ( $\text{N}/\text{m}^3$ )
$f_0$	normal stress ( $\text{N}/\text{m}^2$ )
$I$	acoustic intensity ( $\text{W}/\text{m}^2$ )
$i$	identity matrix
$k$	thermal conductivity ( $\text{W}/(\text{m K})$ )
$n$	normal vector
$p$	pressure ( $\text{N}/\text{m}^2$ )
$Q$	heat source ( $\text{W}/\text{m}^3$ )
$T$	temperature (K)
$u$	velocity ( $\text{m/s}$ )
$t$	time (s)

### Greek letters

$\alpha$	acoustic absorption coefficient ( $\text{m}^{-1}$ )
$\varepsilon_p$	porosity
$\kappa$	permeability ( $\text{m}^2$ )
$\rho$	density ( $\text{kg}/\text{m}^3$ )
$\omega$	angular frequency ( $\text{rad/s}$ )
$\omega_b$	blood perfusion rate ( $1/\text{s}$ )
$\mu$	dynamic viscosity ( $\text{N}\cdot\text{s}/\text{m}^2$ )

### Subscripts

$b$	blood
$ext$	external
$eff$	effective
$met$	metabolic
$n$	normal
$r$	radial coordinate
$s$	solid
$ref$	reference
$z$	axial coordinate

## References

- [1] J.E. Kennedy, High-intensity focused ultrasound in the treatment of solid tumors, *Nat. Rev. Canc.* 5 (2005) 321–327.
- [2] R. Kleinerman, T.B. Whang, R.L. Bard, E.S. Marmor, Ultrasound in dermatology: principles and applications, *J. Am. Acad. Dermatol.* 67 (3) (2012) 478–487.
- [3] H. Park, E. Kim, J. Kim, Y. Ro, J. Ko, High-intensity focused ultrasound for the treatment of wrinkles and skin laxity in seven different facial areas, *Ann. Dermatol.* (2015) 688–693.
- [4] M. Rezaei, K. Khoshgard, M. Mousavi, The correction of focal point displacement caused by the refraction of the beams in high-intensity focused ultrasound, *J. Med. Signal. Sens.* 7 (2017) 178–184.
- [5] P.S. Yarmolenko, E.J. Moon, C. Landon, A. Manzoor, D.W. Hochman, B.L. Vigiante, M.W. Dewhirst, Thresholds for thermal damage to normal tissues: an update, *Int. J. Hyperther.* 27 (4) (2011) 320–343.
- [6] H.H. Pennes, Analysis of tissue and arterial blood temperatures in the resting human forearm, *J. Appl. Physiol.* 1 (1948) 93–122.
- [7] W. Wulff, The energy conservation equation for living tissue, *IEEE Trans. Biomed. Eng.* 21 (6) (1974) 494–495.
- [8] H.G. Klinger, Heat transfer in perfused biological tissue. I: general theory, *Bull. Math. Biol.* 36 (4) (1974) 403–415.
- [9] B. Kundu, D. Dewanjee, A new method for non-Fourier thermal response in a single layer skin tissue, *Case Stud. Therm. Eng.* 5 (2015) 79–88.
- [10] S. Weinbaum, L.M. Jiji, D.E. Lemons, Theory and experiment for the effect of vascular microstructure on surface tissue heat transfer. Part I: anatomical foundation and model conceptualization, *ASME J. Biomech. Eng.* 106 (4) (1984) 321–330.
- [11] C. Chen, L.X. Xu, A vascular model for heat transfer in an isolated pig kidney during water bath heating, *ASME J. Heat Transfer.* 125 (5) (2003) 936–943.
- [12] A. Dhall, A. Halder, A.K. Datta, Multiphase and multicomponent transport with phase change during meat cooking, *J. Food Eng.* 113 (2012) 299–309.
- [13] A. Khalid, I. Khan, A. Khan, S. Shafie, I. Tlili, Case study of MHD blood flow in a porous medium with CNTs and thermal analysis, *Case Stud. Therm. Eng.* 12 (2018) 374–380.
- [14] T.C. Shih, H.L. Liu, K.C. Ju, C.S. Huang, P.Y. Chen, H.W. Huang, Y.J. Ho, The feasibility of heating on tumor periphery by using high intensity focused ultrasound thermal surgery, *Int. Commun. Heat Mass Tran.* 35 (2008) 439–445.
- [15] Y. Li, D. Zeng, J. Tan, Reconstruction of thermal field in target tissue during the therapy of high intensity focused ultrasound, *Int. Commun. Heat Mass Tran.* 108 (2019) 104325.
- [16] A. Bhowmik, R. Repaka, S.C. Mishra, K. Mitra, Thermal assessment of subsurface tumor during focused ultrasound and laser heating, *J. Therm. Sci. Eng. Appl.* 8 (2016), 011012-1.
- [17] T.W.H. Sheu, M.A. Solovchuk, A.W.J. Chen, M. Thiriet, On an acoustics–thermal–fluid coupling model for the prediction of temperature elevation in liver tumor, *Int. J. Heat Mass Tran.* 54 (2011) 4117–4126.
- [18] M.A. Solovchuk, M. Thiriet, T.W.H. Sheu, Computational study of acoustic streaming and heating during acoustic hemostasis, *Appl. Therm. Eng.* 124 (2017) 1112–1122.
- [19] J. Huang, R.G. Holt, R.O. Cleveland, R.A. Roy, Experimental validation of a tractable numerical model for focused ultrasound heating in flow-through tissue phantom, *Acoust. Soc. Am.* 116 (4) (2004) 2451–2458.
- [20] P. Gupta, A. Srivastava, Numerical analysis of thermal response of tissues subjected to high intensity focused ultrasound, *Int. J. Hyperther.* 35 (1) (2018) 419–434.
- [21] P. Gupta, A. Srivastava, Non-Fourier transient thermal analysis of biological tissue phantoms subjected to high intensity focused ultrasound, *Int. J. Heat Mass Tran.* 136 (2019) 1052–1063.
- [22] P. Keangin, T. Wessapan, P. Rattanadecho, Analysis of heat transfer in deformed liver cancer modeling treated using a microwave coaxial antenna, *Appl. Therm. Eng.* 31 (16) (2011) 3243–3254.
- [23] P. Wongchadaku, P. Rattanadecho, T. Wessapan, Implementation of a thermomechanical model to simulate laser heating in shrinkage tissue (effects of wavelength, laser irradiation intensity, and irradiation beam area), *Int. J. Therm. Sci.* 134 (2018) 321–336.
- [24] P. Montienthong, P. Rattanadecho, Focused ultrasound ablation for the treatment of patients with localized deformed breast cancer: computer simulation, *J. Heat Tran.* 141 (10) (2019) 101101.
- [25] T. Wessapan, P. Rattanadecho, Numerical analysis of specific absorption rate and heat transfer in human head subjected to mobile phone radiation, *ASME J. Heat Tran.* 134 (2012) 121101.
- [26] T. Wessapan, S. Srisawatdhisukul, P. Rattanadecho, Specific absorption rate and temperature distributions in human head subjected to mobile phone radiation at different frequencies, *Int. J. Heat Mass Tran.* 55 (2012) 347–359.
- [27] T. Wessapan, P. Rattanadecho, Heat transfer analysis of the human eye during exposure to sauna therapy, *Numer. Heat Tran. Appl.* 68 (2015) 566–582.
- [28] T. Wessapan, P. Rattanadecho, P. Wongchadaku, Effect of the body position on natural convection within the anterior chamber of the human eye during exposure to electromagnetic fields, *Numer. Heat Tran. Appl.* 69 (2016) 1014–1028.
- [29] T. Wessapan, S. Srisawatdhisukul, P. Rattanadecho, Numerical analysis of specific absorption rate and heat transfer in the human body exposed to leakage electromagnetic field at 915 MHz and 2450 MHz, *ASME J. Heat Tran.* 133 (2011), 051101.
- [30] T. Wessapan, S. Srisawatdhisukul, P. Rattanadecho, The effects of dielectric shield on specific absorption rate and heat transfer in the human body exposed to leakage microwave energy, *Int. Commun. Heat Mass Tran.* 38 (2011) 255–262.
- [31] T. Wessapan, P. Rattanadecho, Temperature induced in the testicular and related tissues due to electromagnetic fields exposure at 900 MHz and 1800 MHz, *Int. J. Heat Mass Tran.* 102 (2016) 1130–1140.
- [32] T. Wessapan, P. Rattanadecho, Flow and heat transfer in biological tissue due to electromagnetic near-field exposure effects, *Int. J. Heat Mass Tran.* 97 (2016) 174–184.
- [33] H.C. Brinkman, A calculation of the viscous force exerted by a flowing fluid on a dense swarm of particles, *Appl. Sci. Res.* A1 (1949) 27–34.
- [34] P.A. Hasgall, F. Di Gennaro, C. Baumgartner, E. Neufeld, M.C. Gosselin, D. Payne, A. Klingenböck, N. Kuster, IT'IS Database for thermal and electromagnetic parameters of biological tissues, Version 4.0, May 15th, <http://www.itis.ethz.ch/database>, 2018.
- [35] A. Fahlgren, L. Johansson, U. Edlund, P. Aspenberg, Direct ex vivo measurement of the fluid permeability of loose scar tissue, *Acta Bioeng. Biomech.* 14 (2) (2012) 47–51.